Journal of Solid State Chemistry 183 (2010) 606–612

Contents lists available at ScienceDirect

Journal of Solid State Chemistry

journal homepage: www.elsevier.com/locate/jssc

Synthesis, crystal structure, and properties of the rhombohedral modification of the thiospinel $CuZr_{1.86(1)}S_4$

Yongkwan Dong [a], Michael A. McGuire [b,1], Hoseop Yun [c,*], Francis J. DiSalvo [a,*]

[a] Baker Laboratory, Department of Chemistry, Cornell University, Ithaca, NY 14853-1301, USA
[b] Department of Physics, Cornell University, Ithaca, NY 14853-1301, USA
[c] Division of Energy Research System and Department of Chemistry, Ajou University, Suwon 442-749, South Korea

ARTICLE INFO

Article history:
Received 20 August 2009
Received in revised form
7 December 2009
Accepted 12 December 2009
Available online 23 December 2009

Keywords:
Thiospinel
Semiconductor
Crystal structure
Rhombohedral

ABSTRACT

The rhombohedral modification of the thiospinel, $CuZr_{1.86(1)}S_4$, has been synthesized by the reaction of the constituent elements in an alkali metal halide flux and structurally characterized by single crystal X-ray diffraction techniques. The title compound crystallizes in the rhombohedral space group D_{3d}^5-$R\bar{3}m$ (#166, a=7.3552(2) Å, c=35.832(2) Å, V=1678.76(13) Å^3, Z=12, and R/wR=0.0239/0.0624). The structure is composed of close packed S layers, with a stacking order of ⋯ABCBCABABCACAB⋯⋯along the c axis. The Zr and Cu atoms occupy the octahedral and tetrahedral holes between S layers, respectively. Three different kinds of S-M-S layers exist in the structure: layer I has fully occupied Zr and Cu sites, layer II has fully occupied Zr sites but no Cu, and layer III has partially occupied Zr and fully occupied Cu sites. Transport and optical properties indicate that the title compound is a small band gap (1.26 eV) n-type semiconductor.

1. Introduction

Cubic $MM_2'X_4$ spinels (M and M' = transition metals; X=O, S, Se, or Te) in which the anions X are close packed, the M is in a tetrahedral hole of T_d symmetry, and M' is in an octahedral hole of O_h symmetry (normal spinel), as well as those in which M and M' switch sites (inverse spinel) are well known. Among the many spinel compounds, copper containing thiospinels (CuM_2S_4) have been well investigated due to their unusual physical properties as well as their potential utility as an electrode (cathode) material in rechargeable Li-ion batteries. For instance, CuV_2S_4 shows structural phase transition due to charge density waves at low temperature [1], $CuIr_2S_4$ exhibits a metal-insulator transition at 230 K accompanied by a structural phase transition [2] with a concurrent charge-ordering and spin-dimerization [3], and $CuRh_2S_4$ shows a superconductor-insulator transition under pressure between 5.0 and 5.6 GPa [4]. The crystal structures of $CuTi_2S_4$ and $CuZr_2S_4$ are well known and their physical properties are still under investigation [5–8]. In addition, those compounds were considered as a candidate cathode material in Li-ion batteries because the Cu content can be varied over a wide range [9–14]. Clearly the physical properties of spinel-type compounds depend on their chemical composition and cation arrangement, as well as the temperature and pressure, as noted above.

Recently, a rhombohedral modification of $CuTi_2S_4$ has been synthesized using eutectic alkali metal halide fluxes (KCl/KI) [7]. The usual form of $CuTi_2S_4$ is cubic, but when prepared in a flux at low temperatures, the rhombohedral form is obtained. Interestingly, in the cubic form the Cu–Ti distances are too large for a significant interaction, while in the rhombohedral form that distance is much shorter. Perhaps this interaction plays a role in the stabilization of the later phase. One of the Ti atoms in the rhombohedral $CuTi_2S_4$ has a large displacement parameter but no site deficiency.

In this paper, we report the preparation, single crystal structure, and physical (thermal conductivity, transport, and optical) properties of a Zr deficient rhombohedrally distorted spinel related compound, $CuZr_{1.86(1)}S_4$.

2. Experimental section

2.1. Synthesis

The compound $CuZr_{1.86(1)}S_4$ was prepared by the reaction of elemental Cu, Zr, and S in a RbCl flux. A combination of the elements, Cu powder (CERAC 99.8%), Zr powder (CERAC 99.5%), and S powder (Aldrich 99.9999%), was loaded into a silica tube in the atomic ratio of Cu:Zr:S=1:2:4, and then RbCl was added in a weight ratio of $CuZr_2S_4$:RbCl=1:2. The tube was evacuated to

* Corresponding authors.
E-mail addresses: hsyun@ajou.ac.kr (H. Yun), fjd3@cornell.edu (F.J. DiSalvo).
[1] Materials Science and Technology Division, Oak Ridge National Laboratory, Oak Ridge, Tennessee 37831, USA.

0022-4596/$ - see front matter © 2009 Elsevier Inc. All rights reserved.
doi:10.1016/j.jssc.2009.12.012

$\sim 10^{-3}$ Torr, sealed under vacuum, and heated gradually to 750 °C for 24 h in a muffle furnace, where it was kept for 3 days. The tube was slowly cooled to 100 °C at 4 °C/h and quenched naturally to room temperature in air. After filtering and washing with distilled water to remove the RbCl flux, black shiny plate-like needles up to 0.60 mm in length were found.

A bulk powder sample can be obtained from the stoichiometric reaction of the elements. Cu, Zr, and S were weighed out in a 1:1.86:4 ratios, ground together, and sealed in a silica tube under vacuum. After heating to 750 °C over 24 h, the reaction tube was held at this temperature for 1 day and then slow cooled to 450 °C over 1 day. At this temperature, the reaction tube dwelt an additional 3 days, the furnace power was then turned off and the sample was allowed to cool to room temperature. The resulting powder was ground and pressed into a pellet (approximate size: 7.8 mm diameter, 2.4 mm thickness) in a hardened steel die. This pellet was sealed under vacuum in a silica tube and heated to 750 °C over 24 h and held at this temperature for 12 h. And then this tube slow cooled to 450 °C over 1 day. After dwelling additional 2 days, the furnace power was turned off. The pellet maintained its shape and the resulting product was phase pure by powder X-ray diffraction (Scintag 2000 θ–θ diffractometer) (Fig. 1). To prepare this compound for properties measurement, this powder was again pressed into a pellet and heated following the above procedure. The single crystals and polycrystalline powder produced by the above reactions are not sensitive to air or water. The pellet obtained by the latter reaction is shiny black in color, and it can be maintained in air indefinitely.

2.2. Crystallographic studies

Single crystal X-ray diffraction data were collected on a Bruker X8 Apex II diffractometer equipped with 4 K CCD detector and graphite-monochromatized Mo$K\alpha$ radiation (λ=0.7107 Å). The black needle crystals were manually selected from the reaction mixture, mounted in a drop of polybutene oil sustained in a plastic loop, and placed onto the goniometer in a cold nitrogen stream. Several crystals were selected to check crystal uniformity and the highest quality crystal ($0.37 \times 0.06 \times 0.02$ mm^3) was chosen for collection of a full data set.

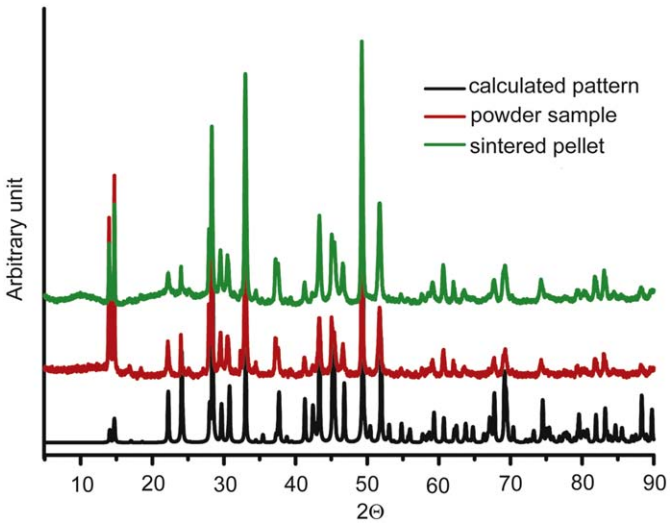

Fig. 1. Powder XRD patterns of the title compound. The black line was calculated from the single crystal data, the red line show as-synthesized powder, and the green line shows the ground powder of the sintered pellet. (For interpretation of the references to color in this figure legend, the reader is referred to the web version of this article.)

The initial unit cell constants and orientation matrix were obtained by using APEX2 [15]. The program SAINT was used to integrate the data [16]. An empirical absorption correction was applied using SADABS [17]. The initial input file for solving the crystal structure was prepared by XPREP [18]. XPREP suggested several possible space groups in the rhombohedral system for the crystal structure. The distribution of normalized structure factor (E-values, $\langle E^2-1\rangle$ =0.963) indicated that the structure should be centrosymmetric. A satisfactory refinement confirmed the choice of space group, $R\bar{3}m$. The initial positions for all atoms were obtained by using direct methods of the SHELXS97 [19] and the structure was refined by full-matrix least-squares techniques with the use of the SHELXL97 [19] in the WinGX [20] program package. Crystal data and further details of data collection are given in Table 1.

The Zr(2) atom has an abnormally large isotropic displacement parameters (IDPs, U_{eq}=0.093 Å^2) and the maximum (5.89 e/Å^3) and minimum (-9.99 e/Å^3) residual peaks are very close to Zr(2) atomic site. This implied that this atom is either disordered over several close sites or that the position is partially occupied. Before refining the site occupancy, wR_2 and R_1 were 0.1789 and 0.0591, respectively. Thus the site occupancy factors of the Zr(2) were refined, while occupancies of other sites were fixed. This resulted in a stoichiometry of $CuZr_{1.857(13)}S_4$. However, the IDP of the Zr(2) atomic site is still a little large (U_{eq}=0.027 Å^2, compared to 0.007 for Zr(1) and Zr(3)). This might be due to data truncation errors ($2\theta \approx 66°$) or to the errors in using an empirical absorption correction for needle-like geometries. In any case the stoichiometry determined by the single crystal diffraction analysis is confirmed by the preparation of a single phase powder at this composition, so we accept the non-stoichiometric formula, $CuZr_{1.86(1)}S4$.

The final cycle of refinement performed on F_o^2 with 787 unique reflections afforded residuals wR_2=0.0624 and a conventional R index based on 753 reflections having $F_o^2 > 2\sigma(F_o^2)$ is 0.0239. The highest peak (1.488 e/Å^3) and deepest hole (-1.424 e/Å^3) in residual electron density are located 0.83 and 1.07 Å from atom

Table 1
Details of X-ray data collection and refinement for $CuZr_{1.86}S_4$.

Formula weight, amu	361.07
Space group	D_{3d}^5-$R\bar{3}m$ (#166)
a, Å	7.3552(2)
c, Å	35.832(2)
V, Å^3	1678.76(13)
Z	12
T, K	167 (5)
Radiation	graphite monochromated Mo$K\alpha$ ($\lambda(K\alpha)$=0.7107 Å)
Density, calc. g/cm^3	4.286
Linear absorption coefficient, mm^{-1}	8.5
Crystal size, mm^3	$0.37 \times 0.06 \times 0.02$
θ limits	$3.25° \le \theta \le 32.79°$
Data collected	$-9 \le h \le 10$, $-9 \le k \le 10$, $-52 \le l \le 47$
Reflections collected / unique (F_o^2)	3886/787 [R(int)=0.0231]
No. of unique data with $F_o^2 > 2\sigma(F_o^2)$	753
Data/restraints/parameters	787/0/37
Goodness-of-fit on F^2	1.260
Final R indices [$F_o^2 > 2\sigma(F_o^2)$][a]	R_1=0.0239, wR_2=0.0621
R indices (all data)[a]	R_1=0.0251, wR_2=0.0624
Extinction coefficient	0.00079(7)
Largest diff. peak and hole	1.488 and -1.424 e/Å^{-3}

w=1/[$\sigma^2(F_o^2)$+(0.0295P)^2+7.2937P] where P=(F_o^2+2F_c^2)/3.

[a] $R_1=\Sigma||F_o|-|F_c||/\Sigma|F_o|$. $wR_2=[\Sigma w(F_o^2-F_c^2)^2/\Sigma(wF_o^2)^2]^{1/2}$.

Table 2
Atomic coordinates and equivalent isotropic displacement parameters (Å^2) for $CuZr_{1.86}S_4$.

Atoms	Wyckoff notation	Site symmetry	x	y	z	Site occupancy (%)	U_{eq}[a]
Cu(1)	6*c*	3*m*	0	0	0.3555(1)	100	0.010(1)
Cu(2)	6*c*	3*m*	0	0	0.1886(1)	100	0.009(1)
Zr(1)	3*a*	−3*m*	0	0	0	100	0.007(1)
Zr(2)	3*b*	−3*m*	0	0	0.5	42.85	0.027(1)
Zr(3)	18*h*	.*m*	0.4956(1)	0.5044(1)	0.4198(1)	100	0.007(1)
S(1)	18*h*	.*m*	0.4952(1)	0.5048(1)	0.1232(1)	100	0.008(1)
S(2)	18*h*	.*m*	0.5062(1)	0.4938(1)	0.2908(1)	100	0.006(1)
S(3)	6*c*	3*m*	0	0	0.2901(1)	100	0.007(1)
S(4)	6*c*	3*m*	0	0	0.1249(1)	100	0.006(1)

[a] U_{eq} is defined as one third of the trace of the orthogonalized U_{ij} tensor.

Table 3
Anisotropic displacement parameters (Å^2) for $CuZr_{1.86}S_4$.

Atoms	U_{11}	U_{22}	U_{33}	U_{23}	U_{13}	U_{12}
Cu(1)	0.009(1)	0.009(1)	0.011(1)	0	0	0.005(1)
Cu(2)	0.009(1)	0.009(1)	0.007(1)	0	0	0.005(1)
Zr(1)	0.007(1)	0.007(1)	0.007(1)	0	0	0.003(1)
Zr(2)	0.027(1)	0.027(1)	0.026(1)	0	0	0.014(1)
Zr(3)	0.007(1)	0.007(1)	0.008(1)	0.000(1)	0.000(1)	0.004(1)
S(1)	0.007(1)	0.007(1)	0.009(1)	0.000(1)	0.000(1)	0.003(1)
S(2)	0.006(1)	0.006(1)	0.007(1)	0.000(1)	0.000(1)	0.003(1)
S(3)	0.007(1)	0.007(1)	0.007(1)	0	0	0.003(1)
S(4)	0.006(1)	0.006(1)	0.006(1)	0	0	0.003(1)

Note: The anisotropic displacement factor exponent takes the form: $-2\pi^2[h^2a^{*2}U_{11}+k^2b^{*2}U_{22}+l^2c^{*2}U_{33}+2klb^*c^*U_{23}+2hla^*c^*U_{13}+2hka^*b^*U_{12}]$.

S(1), respectively. A difference Fourier synthesis calculated with phase and based on the final parameters shows no peak heights greater than 9.3% that of a S atom. The atomic parameters were standardized by using the program STRUCTURE TIDY [21]. Examination of the structure using the ADDSYM algorithm in the PLATON package found no additional symmetry elements [22,23]. Table 2 gives final values of atomic parameters and equivalent isotropic parameters. Final anisotropic displacement parameters appear in Table 3.

2.3. Elemental analysis

A microprobe analysis of the black shiny needle-shaped crystals were made with an EDAX (Thermonoran) equipped scanning electron microscope (JEOL JXA-8900R). Analysis of these crystals showed only the presence of Cu, Zr, and S, and no other impurities which could come from the silica tube or the flux agent were detected. Standardless semi-quantitative analysis gave a Cu/Zr/S atomic percent ratio of 19:29:52 (average of four data acquisitions from two crystals), which is within expected errors of the ratio calculated from the formula $CuZr_{1.86}S_4$ (15:27:58). However, this method is not accurate enough to confirm the Zr deficiency. The composition of the compound was determined to be $CuZr_{2-x}S_4$ (x=0.14) by the single-crystal X-ray diffraction study and the fact that a single phase powder could be prepared at this composition.

2.4. Transport property measurements

Since the compound produced was black in color, suggesting metallic or semiconducting (small band gap) properties, transport measurements were carried out on a polycrystalline pellet. The sintered pellet was cut into a $5.1\times3.3\times2.1\,mm^3$ rectangular bar using a diamond saw for measurements of thermal conductivity κ, thermopower (Seebeck coefficient) S, and electrical resistivity ρ. The thermal conductivity and thermopower were measured simultaneously, while the electrical resistivity was measured during a separate run. All of the measurements were made on the same sample to ensure that they reflect only one doping state of the material. Measurements of transport properties were performed over the temperature range of 80∼300 K under vacuum using a home built apparatus described elsewhere [24]. Contacts to the ends of the bar-shaped sample were made using indium metal, and used for current contact for ρ measurements, and heater/heat sink contacts for S and κ measurements. The voltage contacts for the ρ measurements were made using fine gauge copper wire and silver paste (Dupont Conductor Composition 4922N). Thermocouples for S and κ measurements were attached using silver epoxy (Epotek H20E).

2.5. Solid state UV/Vis spectroscopy

Optical diffuse reflectance measurements were performed at room temperature using a Shimadzu UV-3101PC UV/Vis double beam Spectrophotometer. The instrument is equipped with a 60 mm diameter integrating sphere and controlled by a personal computer. $BaSO_4$ was used as a 100% reflectance standard. A fine powder was prepared by grinding the polycrystalline sample. The powder was then pressed on a compacted surface of the $BaSO_4$ powder preloaded into a sample holder. Reflectance data were collected in the wavelength range 200∼2000 nm and absorption data were calculated from the reflectance data using the Kubelka–Munk funtion: $\alpha/S=(1-R)^2/2R$, where α is the absorption coefficient, S is the scattering coefficient, and R is the reflectance at a given wavelength [25]. The optical band gap was determined as the intersection point between the energy axis at the absorption offset and the line extrapolated from the linear portion of the absorption edge.

2.6. Intercalation chemistry

A detailed description of a home-made apparatus and methodology used has been published elsewhere [26]. The intercalation experiments were carried out inside an argon-filled glovebox to keep an oxygen free environment for the sample and product. For extraction of Cu, a powder sample (∼101 mg) was loaded with I_2 (∼34.4 mg) in 100 ml acetonitrile into a round bottom flask and stirred for 3 days at 62 °C. For intercalation of Cu, a sample (126.6 mg) was mixed with an acetonitrile solution (3 ml) of CuI (12.5 mg), and squeezed between two Cu metal disks in the home-made apparatus [26] in the glovebox for 2 days. A powder diffraction sample of the product obtained from I_2 reaction was prepared in an argon-filled glovebox and covered with Mylar film.

Table 4
Parameters for extended Hückel calculations for $CuZr_2S_4$.

Atoms	Orbital	H_{ii} (eV)	ξ_1	ξ_2	C_1	C_2
Cu	4*s*	−11.40	2.200			
	4*p*	−6.06	2.200			
	3*d*	−14.00	5.950	2.300	0.59332	0.57442
Zr	5*s*	−8.00	1.817			
	5*p*	−5.40	1.776			
	4*d*	−10.20	3.835	1.505	0.62242	0.57822
S	3*s*	−20.000	2.122			
	3*p*	−13.300	1.827			

2.7. Electronic structure calculations

Extended Hückel band structure calculations for the stoichiometric compound $CuZr_2S_4$ were carried out within the tight binding approximation [27,28] at 396 k-point set in the irreducible wedge corresponding to the quarter of 3D Brillouin zone of the rhombohedral system. The CAESAR 2.0 program package [29] was utilized for calculations. The atomic orbital parameters for the EHTB calculation used default values and are listed in Table 4.

3. Results and discussion

The title compound, $CuZr_{1.86(1)}S_4$, crystallizes in the space group $R\bar{3}m$, with two independent positions for Cu, three for Zr, and four for S atoms. This compound is isostructural with the rhombohedral modification of "$CuTi_2S_4$" [7]. Since the copper containing cubic thiospinel compounds (CuM_2S_4) can have a wide range of stoichiometry in Cu as well as *M* [9,11], site occupancy refinement was carried out for all metal sites. We found that only the Zr(2) site has partial occupancy, but it still has an isotropic displacement parameter (U_{eq}=0.027 Å^2) that is about 4 times larger than that of the other Zr atoms. One of the Ti atoms in the rhombohedral $CuTi_2S_4$ [7] also has large displacement parameters even without site deficiency and the large displacement parameters were postulated as due to a *rattling* effect. However, since the Zr(2) site in the title compound is the same as the Ti site in the rhombohedral $CuTi_2S_4$ and is bonded by six equivalent S atoms at the same bond distances, it is difficult to see why this atom should be "rattling" in the octahedral hole more than those in the other zirconium metal sites, Zr(1) and Zr(3).

The projected packing view of the $CuZr_{1.86(1)}S_4$ crystal structure along the [100] direction is illustrated in Fig. 2. The crystal structure is made up of close packed S layers that are staggered along the *c* axis (shown in Fig. 1) and metal atoms (Zr and Cu) partially occupy the octahedral and tetrahedral holes between the S layers. Three different kinds of metal slabs exist in the structure, fully occupied Zr(1) and Cu(1) atoms (Layer I), fully occupied Zr(3) atoms (Layer II), and finally partially occupied Zr(2) atoms and fully occupied Cu(2) (Layer III). Fig. 3 illustrates each layer. The metal layers are similar to the layer sequences of the cubic spinel along the [111] direction, wherein the S atom layers are in a cubic closet packed (···ABC··· sequence). Layer I and III are topologically equivalent to each other. In layer I and III, Zr(1) and Zr(2) atoms are octahedrally coordinated by six S atoms. These octahedra are connected through corner-sharing to Cu(1) and Cu(2) tetrahedra, respectively. The Zr (Zr(1) and Zr(2)) and Cu (Cu(1) and Cu(2)) atoms occupy a quarter of the O_h holes and quarter of the T_d voids of the S atoms, respectively. In layer II, Zr(3) atoms are coordinated by six S atoms in a distorted octahedral environment to form an edge-sharing ZrS_6 chain. The Zr(3) atoms fill three quarters of the O_h holes of the S atoms.

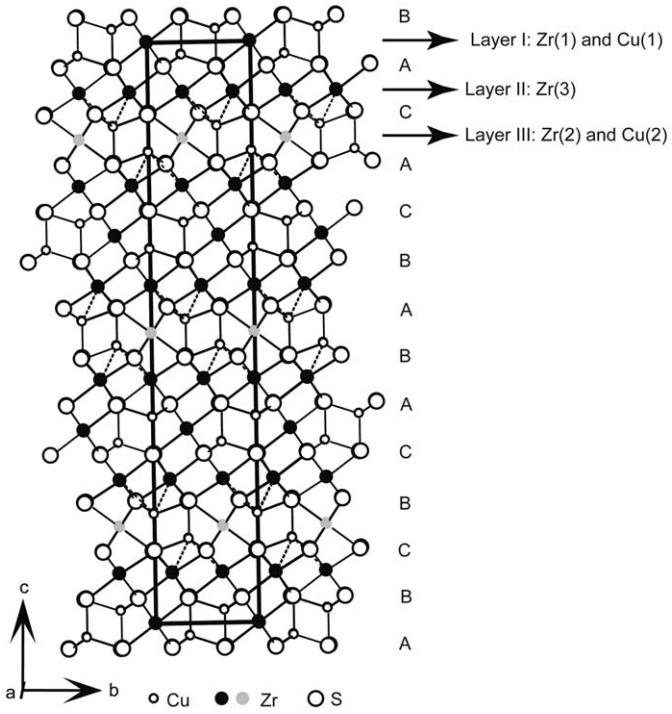

Fig. 2. The projected view of $CuZr_{1.86(1)}S_4$ down the [100] direction. Large letters denote the packing sequence of the S atoms along the *c* axis. The dotted lines indicate the short Cu and Zr interactions. Small open circles are Cu atoms, black circles are Zr(1) and Zr(3) atoms, gray circles are Zr(2) atoms, and large open circles are S atoms.

Overall, the Zr atoms fill half of the O_h holes and the Cu atoms occupy one-eighth of the T_d voids of the closed packed S atoms. Note the occurrence of Cu(2)–Zr(3) distances of 2.9374(5) Å in the rhombohedral form only. (Dotted line in Fig. 2).

Fig. 4 shows the unit cell relationship between cubic and rhombohedral structures. The cubic phase ($CuZr_2S_4$) crystallizes in the $Fd\bar{3}m$ space group with the unit cell dimension a_c=10.378(3) Å [30]. The rhombohedral space group $R\bar{3}m$ is one of the maximal non-isomorphic subgroups of the cubic $Fd\bar{3}m$ space group [31]. Inside the face-centered cubic cell (black solid lines and gray circles), the smallest rhombohedral cell (gray solid lines) can be generated. The *a*- and *c*-axis of the hexagonal representation of the rhombohedral cell (black dashed lines) are seen to be $a_H=(\sqrt{2}/2)a_c$ and $c_H=(\sqrt{3})a_c$, respectively. From the measured data (Table 1), a_H (7.3552(2) Å) is close to $(\sqrt{2}/2)a_c$ (7.338 Å). The value of c_H determined from the cubic cell is 17.975 Å. However, the measured value of the *c* lattice constant is 35.832(2) Å, twice as large as c_H determined from the parent cubic structure. The more complex stacking sequence adopted by this compound, which generates the doubled unit cell, may be related to the non-stoichiometry.

Selected bond distances and angles are listed in Table 5. The Zr–S distances range from 2.5494(7) to 2.5848(7) Å for layer I (Zr(1)) and III (Zr(2)), and from 2.5016(6) to 2.6375(5) Å for layer II (Zr(3) avg. 2.573 Å). Zr(1) and Zr(2) atoms are surrounded by 6 equivalent S atoms (S(2) × 6 for Zr(1) and S(1) × 6 for Zr(2)), while Zr(3) atom is linked by 4 different kinds of S atoms. These values compare to those found in the Zr octahedra compound $CuZr_2S_4$ (2.59 Å) [30] and were roughly comparable to those in the binary sulfide ZrS_2 (2.56 Å) [32]. In the layer I and III, the Zr–Cu and Cu–Cu distances are 4.3317(6) and 4.5448(4) Å for layer I and 4.3303(6) and 4.5393(4) Å for layer III. These imply there are no strong intermetallic bond interactions between the Zr atoms and the Cu atoms. The shortest interlayer Zr–Zr distance is 3.7904(5) Å

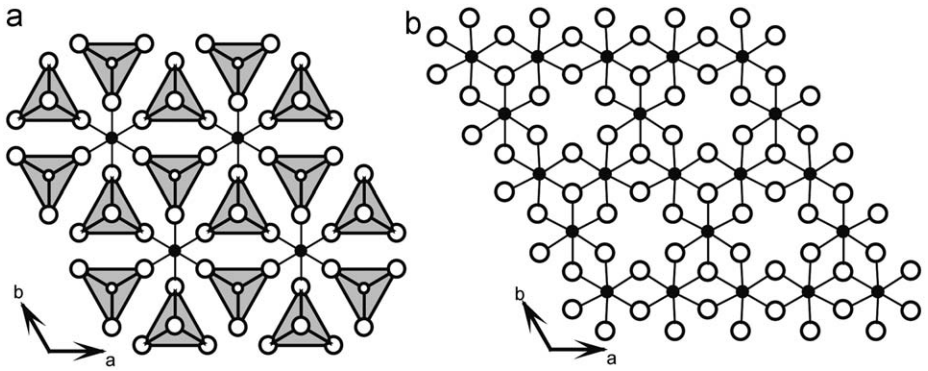

Fig. 3. (a) Layers I and III. Layers I is composed of fully occupied Zr(1) and Cu(1); layer III is made up of partially occupied Zr(2) and fully occupied Cu(2); both Cu(1) and Cu(2) are located in the center of S_4 tetrahedron (b) layer II is made up of fully occupied Zr(3) centered S octahedral. Atoms are as marked in Fig. 2.

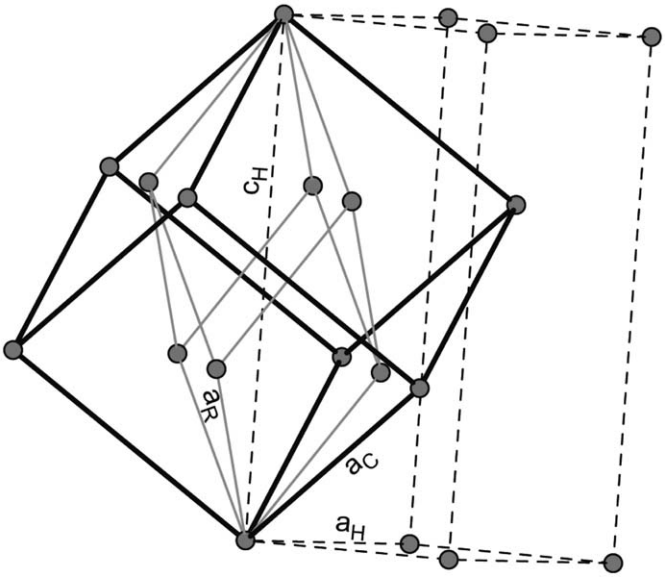

Fig. 4. The relationships between the face-centered cubic lattice (gray circles, black solid lines) and its primitive rhombohedral representation (grey solid lines) and *R*-centered hexagonal representation (black dashed lines). The cubic cell is described by the lattice constant a_C, the hexagonal cell by the lattice constants a_H and c_H, and the rhombohedral cell by the lattice constant a_R and the angle a_R (not shown).

Table 5
Selected bond lengths (Å) for $CuZr_{1.86}S_4$.

Cu(1)–S(2) × 3	2.3196(7)	Cu(2)–S(1) × 3	2.3175(7)
Cu(1)–S(3)	2.3447(14)	Cu(2)–S(4)	2.2841(14)
Cu(2)–Zr(3)	2.9374(5)	Zr(3)–S(1) × 2	2.5016(6)
		Zr(3)–S(2) × 2	2.6375(5)
Zr(1)–S(2) × 6	2.5494(7)	Zr(3)–S(3)	2.5831(8)
Zr(2)–S(1) × 6	2.5848(7)	Zr(3)–S(4)	2.5770(7)

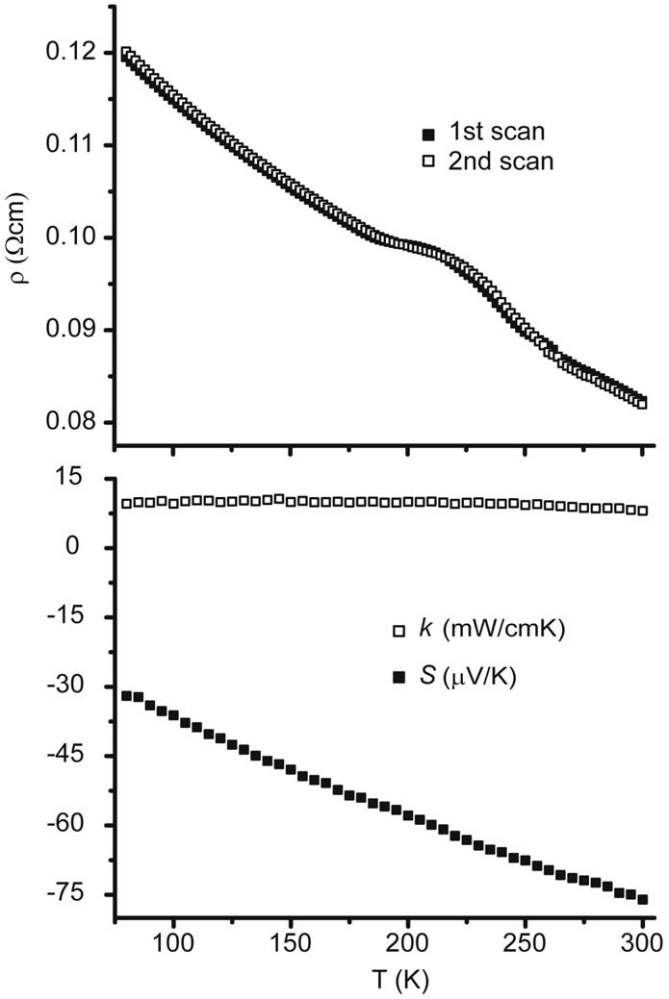

Fig. 5. The measured electrical resistivity ρ, thermopower S, and thermal conductivity κ of $CuZr_{1.86(1)}S_4$.

again indicating no significant metal–metal interaction between metal layers. However, a relatively short Zr(3)–Cu(2) distance (2.9374(5) Å) occurs between layer II and layer III. In the observed stacking sequence, Cu(2) in layer III is in a tetrahedral hole surrounded by three Zr(3) atoms. As a result, the Zr(3) atoms are close to the Cu(2) atoms which generate a relatively short Zr(3)–S(1) distances (2.5016(6) Å). This short copper-transition metal distance is also seen in the rhombohedral modification of $CuTi_2S_4$ [7]. In layer II, the Zr–Zr distances alternate between 3.5908(5) and 3.7848(5) Å. The Cu–S bond lengths range from 2.3196(7) to 2.3447(14) Å (avg. 2.326 Å) for Cu(1) and 2.2841 (14) to 2.3175(7) Å (avg. 2.308 Å) for Cu(2). These values are somewhat larger than those of $CuZr_2S_4$ (2.25 Å) [30] and $CuTi_2S_4$ (avg. 2.27 Å) [7]. However, they are comparable to those found in binary Cu_2S (2.33 Å) [33].

Electrical resistivity, thermopower, and thermal conductivity (Fig. 5) data were obtained from 80 to 300 K for the annealed polycrystalline pellet. The calculated density of the pellet, determined from its mass and dimensions is $\rho = 3.927\ g/cm^3$. The calculated single crystal density is $\rho_{calc.} = 4.286\ g/cm^3$, indicating

that the pellet is about 92% dense. As shown in Fig. 5, the electrical resistivity and thermopower (Seebeck coefficient) decrease with increasing temperature. A reproducible anomaly in the resistivity is observed between 200 and 250 K. The origin of this behavior is unclear at this time, and no corresponding feature is seen in the other transport properties. The resistivity of the title compound is similar to that of the stoichiometric cubic $CuZr_2S_4$ in the measured temperature range [6]. The negative thermopower indicates that the dominant carrier is electrons. Thus the title compound is n-type semiconductor. The thermal conductivity is low and only weakly temperature dependent over the measured temperature range (9.58 mW/cmK at 80 K and 8.07 mW/cmK at 300 K). Although the thermal conductivity is relatively low, the thermoelectric dimensionless figure of merit (ZT) is quite small (0.002 at 300 K) due to the high electrical resistivity and the small Seebeck coefficient.

Electronic structure calculations for stoichiometric $CuZr_2S_4$ were carried out, assuming complete occupancy of the Zr(2) site. In this approximation, the density of states in Fig. 6 was calculated. A total of 516 valence electrons per cell (Z=12; Cu 11×12=132; Zr 4×24=96; S 6×48=288) fill the states up to a Fermi level energy, E_f, of -9.9 eV (black line in Fig. 6). The valence band is dominated by the d states of Cu and s and p states of S, while the d states of Zr atoms contribute mainly to the conduction band. Calculation shows that the stoichiometric compound should be metallic conductor like both the cubic and rhombohedral forms of $CuTi_2S_4$ [6,7]. Assuming we can use a rigid band approximation to estimate the effect of non-stoichiometry, the total number of valence electrons is decreased to 509 (Cu 11×12=132; Zr 4×22.3=89.3; S 6×48=288; total 509.3). This pushes the Fermi level down to -10.05 eV (red line in Fig. 6), which is just at a gap in the density of states. This is consistent with the observed semiconducting behavior.

The bond valence sums were calculated with the program EUTAX [34] and the default values of the R_{ij} for cation–anion single bonds were used to calculate the bond valence sums. The results are listed in Table 6. Previously, Soheilnia et al. [7] postulated that the different oxidation states occur for different

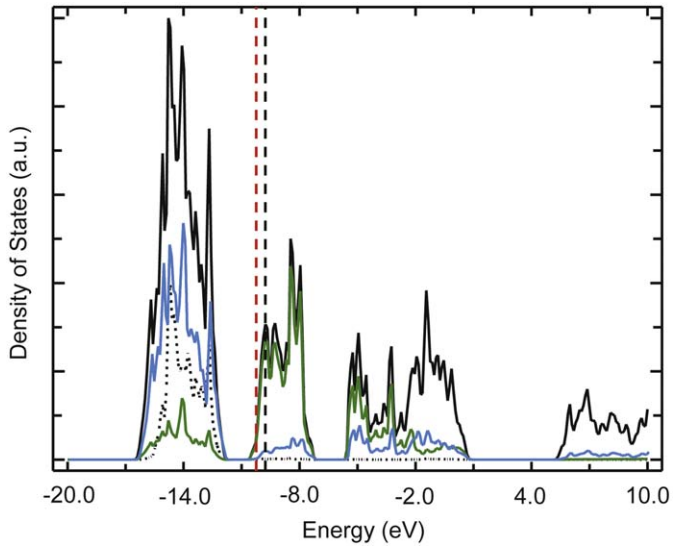

Fig. 6. Density of states of $CuZr_2S_4$ with rhombohedral structure (Solid line is total DOS, black dotted line is d states of Cu atoms, green line is d states of Zr atoms, and blue line is s and p states of S). Black and red dotted lines show the Fermi level of stoichiometric $CuZr_2S_4$ and the estimated Fermi level of non-stoichiometric $CuZr_{1.86(1)}S_4$, respectively. (For interpretation of the references to color in this figure legend, the reader is referred to the web version of this article.)

Table 6
Calculated bond valence sums and Madelung site potentials of $CuZr_{1.86(1)}S_4$.

Atoms	Input charge	Bond valence sum	Madelung site potential (V)
Cu(1)	+1	1.136	−18.411
Cu(2)	+1	1.189	−10.650
Zr(1)	+4	4.117	−31.915
Zr(2)	+3	3.741	−29.750
Zr(3)	+3.5	3.907	−27.762
S(1)	−2	2.476	20.043
S(2)	−2	2.057	19.438
S(3)	−2	2.149	19.363
S(4)	−2	2.228	20.930

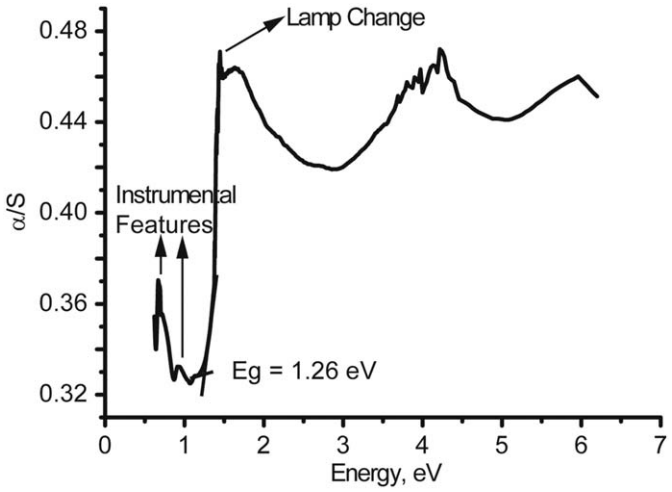

Fig. 7. Solid state UV/Vis spectrum of $CuZr_{1.86}S_4$. The sharp onset at 1.26 eV arises from the optical band gap. Features at lower energies, and just above the gap are instrumental artifacts.

Ti sites in the rhombohedral modification $CuTi_2S_4$ ($(Cu^+)_4$ $Ti1^{4+}Ti2^{3+}(Ti3^{3.5+})_6(S^{2-})_{16}$) according to bond distances (Ti1–S=2.41 Å; Ti2–S=2.52 Å; Ti3–S=avg. 2.41 Å but vary) and electronic structure calculations. Here we use the bond valence sums and the Madelung potentials to explore the possibility of different oxidation states for Zr. To calculate the Madelung site potentials, charges must be assigned to each atom. The oxidation state of Cu atoms in the title compound is assigned +1, consistent with the Cu–S bond distances and the density of states (The d orbital states of Cu atoms are almost zero around E_f). The sulfur is assigned -2, and the Zr assigned as for $CuTi_2S_4$ [7]. Usually, the Madelung potentials are used to confirm the ionic charges assigned for given atoms, since the calculated site potentials are close to -10 times the formal charge of ion [35]. The calculated Madelung potentials and bond valence sums show some difference for the three Zr sites, but nothing as large as that expected for formally Zr^{4+} and Zr^{3+}. These results are consistent with describing the bonding character of the title compound as largely covalent rather than ionic.

The UV/Vis diffuse reflectance spectrum in Fig. 7 was recorded in order to determine the optical band gap of the title compound. The optical band gap was determined as the intersection point between the energy axis and the line extrapolated from the linear potion of the absorption edge in the α/S vs E plots. The obtained value is approximately 1.26 eV. The sharp absorption onset indicates that the title compound has a direct optical band gap; this is in accord with the calculated band structure, which shows a direct band gap at the Γ point. The evaluated optical band gap as

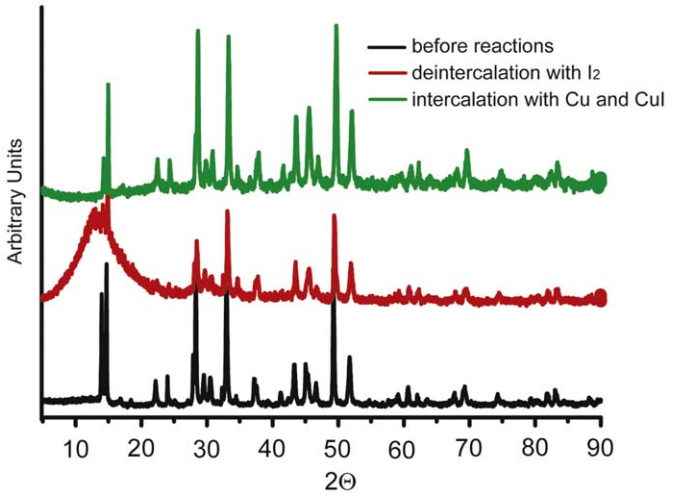

Fig. 8. The PXRD patterns for intercalation study of the title compound, $CuZr_{1.86(1)}S_4$. The broad peak in the red pattern between 10° and 20° is due to a Mylar film that covers the sample. (For interpretation of the references to color in this figure legend, the reader is referred to the web version of this article.)

well as the electrical resistivity corroborates the semiconducting nature of the title compound.

Previous studies of copper chalcogenide spinels suggest that both a copper deficiency and excess are possible [9,11]. Thus intercalation studies were performed for the title compound. As shown in Fig. 8, PXRD patterns show that de-intercalation and intercalation were not successful. The experimental results indicate that this rhombohedral structure differs significantly from other structures obtained by intercalating Cu into the CdI_2 structure of ZrS_2 [36]. In the case of the CdI_2 type ZrS_2, Cu atoms may be inserted into the van der Waals interlayer region of the ZrS_2 layers while retaining the symmetry (using either chemical vapor transport or electrochemical methods) over a wide composition range (Cu_xZrS_2; x=0.1–0.6). It is not clear why intercalation/de-intercalation were not successful. Perhaps higher temperatures are necessary in this case.

4. Conclusions

Single crystal and powder samples of the rhombohedral modification of the thiospinel $CuZr_{1.86(1)}S_4$ have been prepared by using an alkali metal halide flux and conventional solid state synthetic techniques, respectively. Unlike the other metallic cubic and rhombohedral thiospinel (CuM_2S_4; M=group 4 metals), the measured properties show that the title compound is a small band gap n-type semiconductor induced by its non-stoichiometic nature. Hf ($CuHf_2S_4$) and Se/Te ($CuZr_2Q_4$ or $CuHf_2Q_4$) rhombohedral as well as cubic analogues are still unexplored. Since the physical properties of the cubic spinel-type compounds have proved interesting, it would seem profitable to explore the other non-stoichiometric phases in the future.

Supporting information

The crystallographic files in CIF format for the title compounds have been deposited with FIZ Karlsruhe as CSD number 420857 for $CuZr_{1.86(1)}S_4$. The data may be obtained free of charge by contacting FIZ Karlsruhe at +49 7247 808 666 (fax) or crysdata@fiz–karlsruhe.de (email).

Acknowledgments

This work was supported by the National Science Foundation through Grant NSF-DMR-0602526. HY appreciates support by the Korea Research Foundation Grant funded by the Korean Government (MOEHRD) (KFR-2007-412-J04001). We thank Dr E. Lobkovsky (single-crystal diffraction) and J. Hunt (SEM microprobe) for the use of their facilities at Cornell University. The SEM microprobe is available through the Cornell Center for Materials Research Shared Experimental Facilities, supported through the National Science Foundation Materials Research Science and Engineering Center Program (DMR-0079992).

References

[1] R.M. Fleming, F.J. DiSalvo, R.J. Cava, J.V. Waszczak, Phys. Rev. B 24 (1981) 2850–2853.
[2] T. Hagino, T. Tojo, T. Atake, S. Nagata, Philos. Mag. B 71 (1995) 881–894.
[3] P.G. Radaelli, Y. Horibe, M.J. Gutmann, H. Ishibashi, C.H. Chen, R.M. Ibberson, Y. Koyama, Y.-S. Hor, V. Kiryukhin, J.-W. Cheong, Nature 416 (2002) 155–158.
[4] M. Ito, J. Hori, H. Kurisaki, H. Okada, A.J. Perez Kuroki, N. Ogita, M. Udagawa, H. Fujii, F. Nakamura, T. Fujita, T. Suzuki, Phys. Rev. Lett. 91 (2003) 077001.
[5] F.J. DiSalvo, J.V. Wazczak, Phys. Rev. B 26 (1982) 2501–2506.
[6] N. Matsumoto, T. Hagino, K. Taniguchi, S. Chikazawa, S. Nagata, Physica B 284–288 (2000) 1978–1979.
[7] N. Soheilnia, K.M. Kleinke, E. Dashjav, H.L. Cuthbert, J.E. Greedan, H. Kleinke, Inorg. Chem. 43 (2004) 6473–6478 references are there in.
[8] H. Okada, K. Koyama, K. Watanabe, J. Alloys Compd. 403 (2005) 34–37.
[9] S. Sinha, D.W. Murphy, Solid State Ionics 20 (1986) 81–84.
[10] A.C.W.P. James, J.B. Goodenough, Solid State Ionics 27 (1988) 37–43.
[11] A.C.W.P. James, B. Ellis, J.B. Goodenough, Solid State Ionics 27 (1988) 45–55.
[12] M.M. Thackeray, L.A. De Picciotto, A. De Kock, P.J. Johnson, V.A. Nicholas, K.T. Adendorff, J. Power Sources 21 (1987) 1–8.
[13] N. Imanishi, K. Inoue, Y. Takeda, O. Yamamoto, J. Power Sources 44 (1993) 619–625.
[14] V. Bodenez, L. Dupont, M. Morcrette, D.W. Murphy, J.-M. Tarascon, Chem. Mater. 18 (2006) 4278–4287.
[15] Bruker, APEX2 (version 1.22), Software for the CCD System, Bruker Analytical X-ray System, Madison, WI, 2004.
[16] Bruker, SAINT-Plus, Bruker Analytical X-ray Instruments, Inc., Madison, WI, 2003.
[17] G.M. Sheldrick, SADABS, Program for Absorption Correction, Bruker Analytical X-ray Instruments, Inc., Madison, 2003.
[18] Bruker, XPREP (version 6.14): Bruker Analytical X-ray Instruments, Inc, Madison, WI, 2003.
[19] G.M. Sheldrick, SHELX97, Program for the Refinement of Crystal Structure, University of Göttingen, Göttingen, Germany, 1997.
[20] L.J. Farrugia, J. Appl. Crystallogr. 32 (1999) 837–838.
[21] L.M. Gelato, E. Parthé, J. Appl. Crystallogr. 20 (1987) 139–143.
[22] Y. Le Page, J. Appl. Crystallogr. 20 (1987) 264–269;
Y. Le Page, J. Appl. Crystallogr. 21 (1988) 983–984.
[23] A.L. Spek, PLATON. A Multipurpose Crystallographic Tool. Utrecht University, Utrecht, The Netherlands, 1999.
[24] T.K. Reynolds, M.A. McGuire, F.J. DiSalvo, J. Solid State Chem. 177 (2004) 2998–3006.
[25] G. Kortüm, Reflectance Spectroscopy, Springer, New York, 1969.
[26] M.A. McGuire, C. Ranjan, F.J. DiSalvo, Inorg. Chem. 45 (2006) 2718–2726.
[27] R. Hoffmann, J. Chem. Phys. 39 (1963) 1397–1412.
[28] M.-H. Whangbo, R. Hoffmann, J. Am. Chem. Soc. 100 (1978) 6093–6098.
[29] J. Ren, W. Liang, M.-H. Whangbo, CAESER 2.0; Prime Color Software Inc., North Carolina State University, Releigh, NC, 2002.
[30] L. Trichet, J. Rouxel, C. R. Acad. Sci. Ser. C, Sci. Chim. 267 (1968) 1322–1324.
[31] Th. Hahn, International table for crystallography, Vol. A space-group symmetry, fifth ed., The International Union of Crystallography, 2006.
[32] G. Haegg, N. Schoenberg, Arki. Kemi 7 (1954) 371–380.
[33] M. Oliveria, R.K. McMullan, B.J. Wuensch, Solid State Ionics (1988) 1332–1337.
[34] N.E. Brese, M. O'Keeffe, Acta Crystallogr. B 47 (1991) 192–197.
[35] N.E. Brese, M. O'Keeffe, Struct. Bond 79 (1992) 307–379.
[36] F.W. Boswell, B.G. Yacobi, J.M. Corbett, Mater. Res. Bull. (1979) 1111–1118.